HAT-P-30b: A TRANSITING HOT JUPITER ON A HIGHLY OBLIQUE ORBIT

Citation: Johnson, John Asher et al. "HAT-P-30b: A TRANSITING HOT JUPITER ON A HIGHLY OBLIQUE ORBIT." The Astrophysical Journal 735.1 (2011): 24. Web.

As Published: http://dx.doi.org/10.1088/0004-637x/735/1/24

Publisher: Institute of Physics Publishing

Persistent URL: http://hdl.handle.net/1721.1/72417

Version: Author's final manuscript: final author's manuscript post peer review, without publisher's formatting or copy editing

Massachusetts Institute of Technology

HAT-P-30b: A TRANSITING HOT JUPITER ON A HIGHLY OBLIQUE ORBIT [†]

JOHN ASHER JOHNSON[1], J. N. WINN[2], G. Á. BAKOS[3], J. D. HARTMAN[3], T. D. MORTON[1], G. TORRES[3], GÉZA KOVÁCS[4],
D. W. LATHAM[3], R. W. NOYES[3], B. SATO[5], G. A. ESQUERDO[3], D. A. FISCHER[6], G. W. MARCY[7], A. W. HOWARD[7],
L. A. BUCHHAVE[8], G. FŰRÉSZ[3], S. N. QUINN[3], B. BÉKY[3], D. D. SASSELOV[3], R. P. STEFANIK[3], J. LÁZÁR[9], I. PAPP[9],
P. SÁRI[9],

Draft version March 22, 2011

ABSTRACT

We report the discovery of HAT-P-30b, a transiting exoplanet orbiting the V=10.419 dwarf star GSC 0208-00722. The planet has a period $P = 2.810595 \pm 0.000005$ d, transit epoch $T_c = 2455456.46561 \pm 0.00037$ (BJD), and transit duration 0.0887 ± 0.0015 d. The host star has a mass of $1.24 \pm 0.04\,M_\odot$, radius of $1.21 \pm 0.05\,R_\odot$, effective temperature 6304 ± 88 K, and metallicity [Fe/H] $= +0.13 \pm 0.08$. The planetary companion has a mass of $0.711 \pm 0.028\,M_J$, and radius of $1.340 \pm 0.065\,R_J$ yielding a mean density of 0.37 ± 0.05 g cm^{-3}. We also present radial velocity measurements that were obtained throughout a transit that exhibit the Rossiter-McLaughlin effect. By modeling this effect we measure an angle of $\lambda = 73.5° \pm 9.0°$ between the sky projections of the planet's orbit normal and the star's spin axis. HAT-P-30b represents another example of a close-in planet on a highly tilted orbit, and conforms to the previously noted pattern that tilted orbits are more common around stars with $T_{\rm eff\star} \gtrsim 6250$ K.

Subject headings: planetary systems — stars: individual (HAT-P-30, GSC 0208-00722) techniques: spectroscopic, photometric

1. INTRODUCTION

The majority of known exoplanets have been discovered either by detecting the gravitational pull of a planet on its central star using Doppler spectroscopy, or by observing the small decrement in flux from the star during a transit of its planet. The two techniques are complementary: several Doppler-detected planets have later been found to transit (Henry et al. 2000; Charbonneau et al. 2000), while those systems initially detected through photometric surveillance require Doppler follow-up observations to confirm the planet's existence (e.g. Bakos et al. 2007).

The combination of Doppler-shift measurements and transits can also reveal an interesting aspect of the planetary system's architecture: the orientation of the planet's orbital plane with respect to the star's spin axis. This is

[1] California Institute of Technology, Department of Astrophysics, MC 249-17, Pasadena, CA 91125; NASA Exoplanet Science Institute (NExScI)
[2] Department of Physics, and Kavli Institute for Astrophysics and Space Research, Massachusetts Institute of Technology, Cambridge, MA 02139
[3] Harvard-Smithsonian Center for Astrophysics, Cambridge, MA; email: gbakos@cfa.harvard.edu
[4] Konkoly Observatory, Budapest, Hungary.
[5] Department of Earth and Planetary Sciences, Tokyo Institute of Technology, 2-12-1 Ookayama, Meguro-ku, Tokyo 152-8551
[6] Department of Astronomy, Yale University, New Haven, CT
[7] Department of Astronomy, University of California, Berkeley, CA
[8] Niels Bohr Institute, Copenhagen University, DK-2100 Copenhagen, Denmark
[9] Hungarian Astronomical Association, Budapest, Hungary
[†] Based in part on observations obtained at the W. M. Keck Observatory, which is operated by the University of California and the California Institute of Technology. Keck time has been granted by NASA (N167Hr). Based in part on data collected at Subaru Telescope, which is operated by the National Astronomical Observatory of Japan.

done by measuring the apparent Doppler shift of the star throughout a transit. As the planet's shadow traverses the rotating stellar surface it alternately blocks the approaching and receding limbs, giving rise to anomalous Doppler shift known as the Rossiter-McLaughlin effect (Rossiter 1924; McLaughlin 1924). By modeling this effect one may determine the angle λ on the sky between the angular momentum vectors of the planetary orbit and the stellar spin (Queloz et al. 2000; Ohta et al. 2005; Winn et al. 2005; Gaudi & Winn 2007).

The spin-orbit angles observed among transiting planets have provided clues about the processes that give rise to the population of close-in planets. Giant exoplanets are thought to have formed on wide orbits and subsequently moved inward to smaller semimajor axes through a process generically known as orbital migration. There are many theories for the mechanisms of inward migration, and each process leaves behind clues imprinted in the distribution of λ observed among close-in planetary systems.

The initial spin-orbit measurements indicated that the majority of systems are well-aligned (e.g. Winn et al. 2005), and this finding supported the notion that planets likely migrated through a mechanism such as Type II disk migration that preserves, or even enforces, a close alignment between the planet orbit normal and stellar spin axis (Winn et al. 2006; Johnson et al. 2008; Fabrycky & Winn 2009). However, a larger collection of spin-orbit measurements has revealed that misaligned, and even retrograde systems are quite common (Hébrard et al. 2008; Winn et al. 2009; Johnson et al. 2009; Anderson et al. 2010; Triaud et al. 2010; Morton & Johnson 2011). It now appears that disk migration is not the only migration channel, and that impulsive, gravitational interactions are likely responsible for forming many of the known close-in planetary
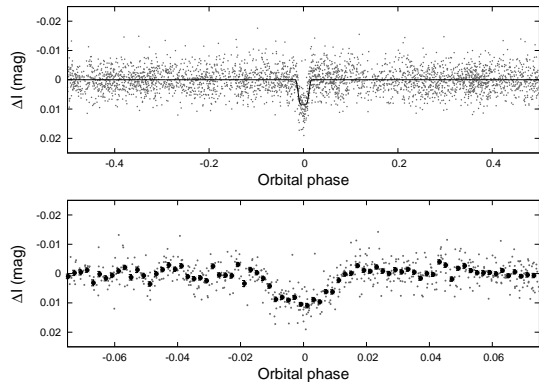
FIG. 1.— Unbinned light curve of HAT-P-30, including ≈3200 data points obtained with the HAT-5 and HAT-9 telescopes of HATNet in the instrumental I_C band with a 5.5-minute cadence (see the text for details). The data have been folded with the period $P = 2.8105951$ days resulting from the global fit described in Section 3). The solid line shows a simplified transit model fit to the light curve (Section 3.2). The bottom panel shows a zoomed-in view of the transit, the filled circles show the light curve binned in phase with a bin-size of 0.002.

systems.

Winn et al. (2010) noted that the misaligned planets tended to be those having the hottest host stars ($T_{\text{eff}\star} > 6250\,K$). They suggested that this is a signal that planet migration operates differently for stars of differing masses. Another hypothesis put forth by Winn et al. (2010) is that cool stars are observed to have low obliquities only because of tidal interactions between the close-in planet and the star's relatively thick convective envelope, while hotter stars have thinner outer envelopes and weaker tidal dissipation. Indeed, Morton & Johnson (2011) found that the collection of λ measurements for 12 systems containing hot stars was consistent with all systems being misaligned[11]. If this interpretation proves to be correct then the hot stars are giving a clearer picture of the migration mechanism and its resulting distribution of angular momentum, while the cooler stars have been affected by subsequent tidal evolution.

To detect the Rossiter-McLaughlin effect and measure the spin-orbit angle typically requires a time series of Doppler-shift measurements with a precision of order 1–10 m s^{-1} and a time sampling of about 15 min or better. While the space-based transit survey mission, *Kepler*, has recently increased the sample of known transiting systems by an order of magnitude (Borucki et al. 2011), only the very brightest stars in the *Kepler* sample are amenable to precise measurement of λ (e.g. Jenkins et al. 2010). Ground-based transit surveys thus play a valuable role in understanding exoplanet characteristics by providing additional, bright ($V < 12$) systems amenable to high-resolution, spectroscopic follow up.

In this contribution, we announce the discovery of a new transiting planet orbiting a bright, early-type star, which represents the thirtieth planet detected by the Hungarian-made Automatic Telescope Network (HATNet; Bakos et al. 2004). For this system we also observed the Rossiter-McLaughlin effect, and found that the host

[11] The measurement of λ represents the sky-projected spin-orbit angle, not the true 3-dimensional angle ψ. Thus, the fraction of truly misaligned requires a statistical deprojection (e.g. Fabrycky & Winn 2009).

star HAT-P-30 is a member of the growing collection of hot stars with highly-tilted hot Jupiters.
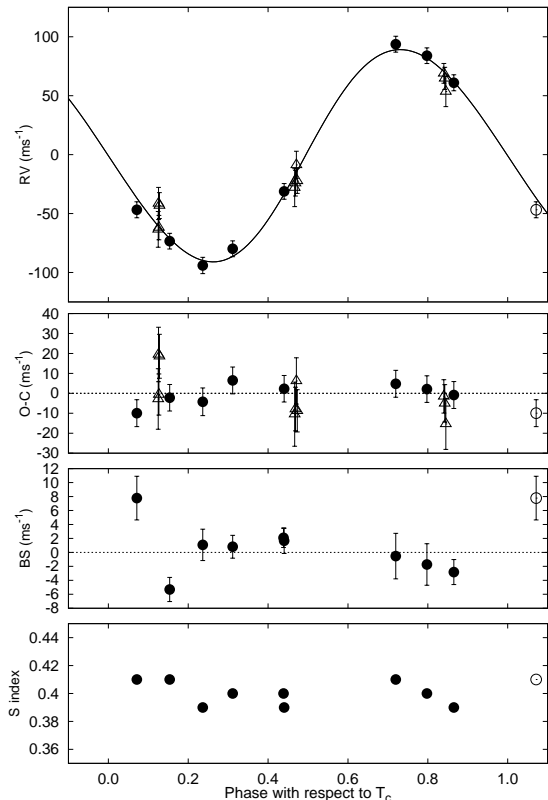

FIG. 2.— *Top panel:* Keck/HIRES RV measurements (filled circles) and Subaru/HDS RV measurements (open triangles) for HAT-P-30 shown as a function of orbital phase, along with our best-fit model (see Table 4). Zero phase corresponds to the time of mid-transit. The center-of-mass velocity has been subtracted. *Second panel:* Velocity $O-C$ residuals from the best fit. The error bars include a component from astrophysical/instrumental jitter (6.3 m s^{-1} for HIRES and 2.1 m s^{-1} for HDS) added in quadrature to the formal errors such that $\chi^2_\nu = 1$ (see Section 3.2). *Third panel:* Bisector spans (BS) for the HIRES spectra, with the mean value subtracted, and the measurement from the template spectrum is included. *Bottom panel:* Chromospheric activity index S measured from the Keck spectra. Note the different vertical scales of the panels. Observations shown twice are represented with open circles.

2. OBSERVATIONS

The HATNet observing strategy has been described in detail in previous articles (e.g. Bakos et al. 2010; Latham et al. 2009), and we summarize it briefly as follows. Photometric observations with one or more of the HATNet telescopes initially identify stars exhibiting periodic dimming events that resemble the signals of planetary transits. These candidates are then followed up using high-resolution, low-S/N "reconnaissance" spectroscopic observations using 1-2 m class telescopes. The spectroscopic observations allow many false positives to be rejected (e.g. unresolved blends of bright stars with background eclipsing binaries). Additional transit light curves are acquired to refine the light curve properties. Finally, high-resolution, high-S/N "characterization" spectroscopy is undertaken, with the goals of detecting the orbital motion of the star due to the planet,

TABLE 1
RELATIVE RADIAL VELOCITIES, BISECTOR SPANS, AND ACTIVITY INDEX MEASUREMENTS OF
HAT-P-30.

BJD[a] (2,454,000+)	RV[b] $(\mathrm{m\,s^{-1}})$	σ_{RV}[c] $(\mathrm{m\,s^{-1}})$	BS $(\mathrm{m\,s^{-1}})$	σ_{BS} $(\mathrm{m\,s^{-1}})$	S[d]	Phase	Instrument
1313.78961	−95.85	3.34	1.08	2.25	0.1250	0.236	Keck
1320.76920	84.53	3.11	−0.53	3.26	0.1280	0.720	Keck
1321.75751	−48.39	3.23	7.78	3.13	0.1310	0.071	Keck
1338.77142	−63.42	15.02	⋯	⋯	⋯	0.125	Subaru
1338.77361	−41.42	13.48	⋯	⋯	⋯	0.126	Subaru
1338.77647	−61.91	10.11	⋯	⋯	⋯	0.127	Subaru
1338.78003	−43.23	10.80	⋯	⋯	⋯	0.128	Subaru
1339.73204	−28.01	15.95	⋯	⋯	⋯	0.467	Subaru
1339.73757	−24.22	10.72	⋯	⋯	⋯	0.469	Subaru
1339.74390	−8.72	11.41	⋯	⋯	⋯	0.471	Subaru
1339.75024	−22.31	10.37	⋯	⋯	⋯	0.473	Subaru

NOTE. — For the iodine-free template exposures there is no RV measurement, but the BS and S index can still be determined. This table is presented in its entirety in the electronic edition of the Astrophysical Journal. A portion is shown here for guidance regarding its form and content.
[a] Barycentric Julian dates throughout the paper are calculated from Coordinated Universal Time (UTC).
[b] The zero-point of these velocities is arbitrary. An overall offset γ_{rel} fitted to these velocities in Section 3.2 has *not* been subtracted.
[c] Internal errors excluding the component of astrophysical/instrumental jitter considered in Section 3.2.
[d] Chromospheric activity index, calibrated to the scale of Isaacson & Fischer (2010).

characterizing the host star, and ruling out subtle blend scenarios by detecting line bisector variations. In the following subsections we highlight specific details of this procedure that are pertinent to the discovery of HAT-P-30b.

2.1. Photometric detection

The transits of HAT-P-30 (=GSC 0208-00722) were detected with the HAT-5 telescope in Arizona and the HAT-9 telescope in Hawaii, within a target field internally labeled as 364. The field was observed nightly between 2008 December and 2009 May, whenever weather conditions permitted. We gathered 3686 images, each with an exposure time of 5 minutes, and an observing cadence of 5.5 minutes. Approximately 500 images were rejected by our reduction pipeline because they were of relatively poor quality. Each image encompasses about 66,000 stars with r magnitudes brighter than 14.5. For the brightest stars in the field, we achieved a per-image photometric precision of 4 mmag.

The HATNet images were calibrated, and trend-filtered light curves were derived for stars in the Two Micron All Sky Survey catalog (2MASS; Skrutskie et al. 2006) following the procedure described by Pál & Bakos (2006); Pál (2009b). We searched the photometric time series of each target using the Box Least-Squares (BLS; Kovács et al. 2002) method. We detected a significant signal in the light curve of GSC 0208-00722 ($\alpha = 08^{\mathrm{h}}15^{\mathrm{m}}47.99\mathrm{s}$, $\delta = +05°50'12.2''$; J2000; V=10.419 Droege et al. 2006), with an apparent depth of ~ 8.8 mmag, and a period of $P = 2.8106$ days (see Figure 1). This star is henceforth referred to as HAT-P-30.

2.2. Reconnaissance Spectroscopy

Four spectra of HAT-P-30 were obtained with the Tillinghast Reflector Echelle Spectrograph (Fűrész 2008) in March 2010, for an initial reconnaissance of the candidate, and thus were not particularly strong exposures;

the typical SNR per resolution element was 50 near the Mg b features. Classification of these spectra using techniques similar to those described by Latham et al. (2009) showed that the star is a slowly-rotating early G dwarf with sharp lines suitable for very precise radial velocities. Multi-order relative radial velocities were derived using the techniques described by Buchhave et al. (2010). A template for the cross-correlations analysis was created by shifting and co-adding the four individual observations to a common velocity.

A circular orbit with the period and phase set by the photometric ephemeris yielded a good fit with semi-amplitude $K = 84.5 \pm 9.8\,\mathrm{m\,s^{-1}}$. This was interpreted as strong evidence that the companion is a Hot Jupiter, and therefore HAT-P-30 was scheduled for additional high-resolution spectroscopic observations with large telescopes to provide a higher-quality orbital solution and more precise mass determination, as described in § 2.3.

2.3. High resolution, high S/N spectroscopy

We proceeded with the follow-up of this candidate by obtaining high-resolution, high-S/N spectra to measure the spectroscopic orbit of the system, and refine the physical parameters of the host star. For this we used the High-Resolution Echelle Spectrometer on the Keck I telescope (HIRES; Vogt et al. 1994), and the High-Dispersion Spectrograph (HDS; Noguchi et al. 2002) on the Subaru telescope, both atop Mauna Kea in Hawaii. For both telescope/spectrometer configurations we used the iodine cell method, which has been described by Marcy & Butler (1992) and Butler et al. (1996). The Keck implementation of this method has been described by Howard et al. (2010) and Johnson et al. (2009), and the Subaru implementation has been described by Sato et al. (2002, 2005). The resulting RV measurements and their uncertainties are listed in Table 1, and the phase-folded RV measurements and best
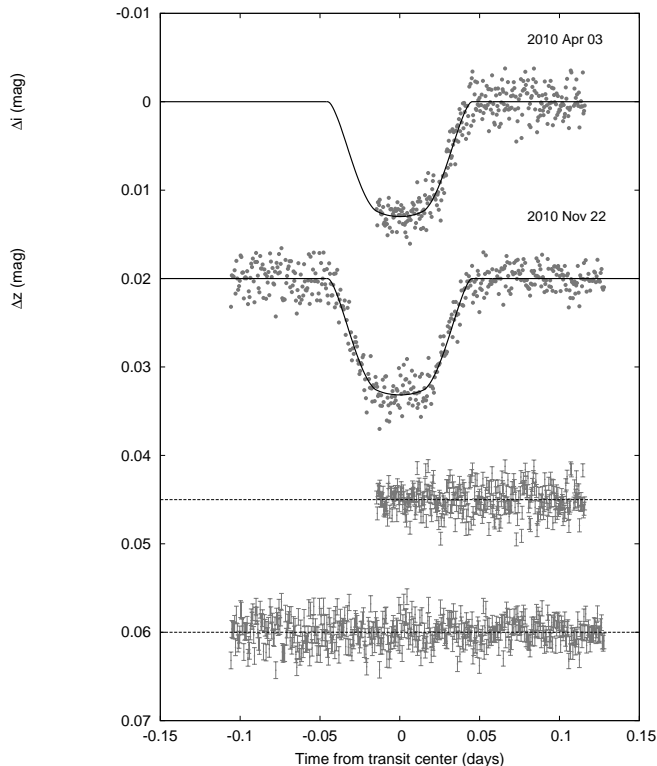
FIG. 3.— Unbinned instrumental i band and z band transit light curves, acquired with KeplerCam at the FLWO 1.2 m telescope. The light curves are displaced vertically for clarity. Our best fit from the global modeling described in Section 3.2 is shown by the solid lines. Residuals from the fits are displayed at the bottom, in the same order as the top curves.

fitting orbit are shown in Figure 2 (see also Section 3).

We also checked if the measured radial velocities are not real, but are instead caused by distortions in the spectral line profiles due to contamination from an unresolved eclipsing binary (e.g. Torres et al. 2007). We performed a bisector analysis on the Keck spectra using the method described in § 5 of Bakos et al. (2007). The resulting bisector spans show no significant variation and are not correlated with the RVs (Figure 2), which argues against false-positive scenarios involving a blended, background eclipsing binary system.

There is no sign of emission in the cores of the Ca II H and K lines in any of our spectra, from which we conclude that the chromospheric activity level in HAT-P-30 is very low and that the star is fairly old (> 1 Gyr). In Figure 2 we also show the S index (Vaughan, Preston & Wilson 1978; Isaacson & Fischer 2010), which is a measure of the chromospheric activity of the star derived from the cores of the Ca II H and K lines. We do not detect significant variation of the index as a function of orbital phase. It is therefore unlikely that the observed RV variations are due to stellar activity.

2.4. Photometric follow-up observations

We acquired additional light curves using the Kepler-Cam imager on the 1.2 m telescope at the Fred Lawrence Whipple Observatory (FLWO). We observed a partial transit on UT 2010 April 3 through the a Sloan i band filter, and a full transit on UT 2010 November 22 using a z band filter. The reduction of the images, including

BJD (2,400,000+)	Mag[a]	$\sigma_{\rm Mag}$	Mag(orig)[b]	Filter
55290.62596	0.01214	0.00073	9.28160	i
55290.62636	0.01398	0.00073	9.28349	i
55290.62675	0.01138	0.00073	9.28059	i
55290.62715	0.01136	0.00073	9.28017	i
55290.62754	0.01169	0.00073	9.28064	i
55290.62793	0.01108	0.00073	9.28062	i
55290.62833	0.01237	0.00073	9.28116	i
55290.62871	0.01269	0.00073	9.28152	i
55290.62911	0.01274	0.00073	9.28093	i
55290.62948	0.01261	0.00073	9.28249	i

NOTE. — This table is available in a machine-readable form in the online journal. A portion is shown here for guidance regarding its form and content.
[a] The out-of-transit level has been subtracted. These magnitudes have been subjected to the EPD and TFA procedures.
[b] Raw magnitude values without application of the EPD and TFA procedures.

basic calibration, astrometry, and aperture photometry, was performed as described by Bakos et al. (2010) The final time series are shown in the top portion of Figure 3, along with our best-fit transit light curve model described below; the individual measurements are reported in Table 2.

3. ANALYSIS

The analysis of the HAT-P-30 system, including determinations of the properties of the host star and planet, was carried out in a similar fashion to previous HAT-Net discoveries (e.g. Bakos et al. 2010). Below we briefly summarize the procedure and the results for the HAT-P-30b system.

3.1. Properties of the parent star

We estimate stellar atmospheric parameters based on the iodine-free "template" spectrum of the star obtained with the Keck/HIRES instrument. We fitted the spectra using synthetic spectra generated by the LTE analysis package known as Spectroscopy Made Easy (SME; Valenti & Piskunov 1996), with the atomic line database of Valenti & Fischer (2005). SME provides the following initial values and uncertainties: effective temperature $T_{\rm eff\star} = 6169 \pm 100\,$K, metallicity [Fe/H] $= +0.06 \pm 0.1\,$dex, and stellar surface gravity $\log g_\star = 4.18 \pm 0.06\,$(cgs), projected rotational velocity $v \sin i = 2.9 \pm 0.5\,$km s^{-1}.

We use these parameters to determine the limb-darkening coefficients needed in the global modeling of the follow-up photometry. This modeling strongly constrains the stellar density $\rho_\star$, which combined with the spectroscopically determined $T_{\rm eff\star}$ and [Fe/H] and the Yonsei-Yale stellar evolution models (YY; Yi et al. 2001) provides a refined estimate of $\log g_\star$. We perform a second iteration of SME with $\log g_\star$ fixed to this value, followed by a second iteration of the global modeling and comparison to the YY models. The resulting $\log g_\star$ was consistent with the previous value so that no further iterations of this procedure were needed. Our final adopted stellar parameters are listed in Table 3. We find that HAT-P-30 is a Gyr-old F-type dwarf star with a mass of

Parameter	Value	Source
Spectroscopic properties		
$T_{\mathrm{eff}\star}$ (K)	6304 ± 88	SME[a]
[Fe/H]	$+0.13 \pm 0.08$	SME
$v \sin i$ (km s^{-1}) ...	2.2 ± 0.5	SME
v_{mac} (km s^{-1})	4.84	SME
v_{mic} (km s^{-1})	0.85	SME
γ_{RV} (km s^{-1})	45.51 ± 0.18	TRES
Photometric properties		
V (mag)..........	10.419	TASS
$V - I_C$ (mag)	0.527 ± 0.12	TASS
J (mag)	9.442 ± 0.026	2MASS
H (mag)	9.220 ± 0.028	2MASS
K_s (mag)	9.151 ± 0.023	2MASS
Derived properties		
$M_\star$ ($M_\odot$)	1.242 ± 0.041	YY+$a/R_\star$+SME [b]
$R_\star$ ($R_\odot$)	1.215 ± 0.051	YY+$a/R_\star$+SME
$\log g_\star$ (cgs)	4.36 ± 0.03	YY+$a/R_\star$+SME
$L_\star$ ($L_\odot$)	2.05 ± 0.24	YY+$a/R_\star$+SME
M_V (mag)........	3.98 ± 0.14	YY+$a/R_\star$+SME
M_K (mag,ESO) ..	2.77 ± 0.10	YY+$a/R_\star$+SME
Age (Gyr)	$1.0^{+0.8}_{-0.5}$	YY+$a/R_\star$+SME
Distance (pc)	193 ± 8	YY+$a/R_\star$+SME+2MASS

[a] SME = "Spectroscopy Made Easy" package for the analysis of high-resolution spectra (Valenti & Piskunov 1996). These parameters rely primarily on SME, but have a small dependence also on the iterative analysis incorporating the isochrone search and global modeling of the data, as described in the text.
[b] YY+$a/R_\star$+SME = Based on the YY isochrones (Yi et al. 2001), $a/R_\star$ as a luminosity indicator, and the SME results.

$M_\star = 1.24 \pm 0.04 M_\odot$ and radius of $R_\star = 1.21 \pm 0.05 R_\odot$.

3.2. *Global modeling of the data*

We modeled the HATNet photometry and follow-up RV measurements using the procedure described in detail by Bakos et al. (2010). The resulting parameters pertaining to the light curves and RV curves, together with derived physical parameters of the planet, are listed in Table 4.

Based on the amplitude of the RV variations, together with the stellar mass and its associated uncertainty, we estimate a mass for the planet of $M_p = 0.711 \pm 0.028\ M_{\mathrm{J}}$. The transit parameters give a planetary radius of $R_p = 1.340 \pm 0.065\ R_{\mathrm{J}}$, leading to a mean planetary density $\rho_p = 0.37 \pm 0.05\ \mathrm{g\,cm^{-3}}$. These and other planetary parameters are listed at the bottom of Table 4. We note that the eccentricity of the orbit is consistent with zero: $e = 0.035 \pm 0.024$, $\omega = 252 \pm 84°$.

3.3. *The Rossiter-McLaughlin effect*

We undertook a separate analysis of the RVs obtained on the transit night (2011 Feb 21) in order to determine the projected spin-orbit angle λ. Our model for the RV data was the sum of the orbital radial velocity, the anomalous velocity due to the Rossiter-McLaughlin effect, and a constant offset:

$$V_{\mathrm{calc}}(t) = V_{\mathrm{orb}}(t) + V_{\mathrm{RM}}(t) + \gamma. \qquad (1)$$

For modeling the RM effect we used the technique of Winn et al. (2005), in which simulated spectra exhibiting the RM effect are created and then analyzed using the

Parameter	Value
Light curve parameters	
P (days)	2.810595 ± 0.000005
T_c (BJD) [a]	$2455456.46561 \pm 0.00037$
T_{14} (days) [a]	0.0887 ± 0.0015
$T_{12} = T_{34}$ (days) [a]	0.0295 ± 0.0025
$a/R_\star$	7.42 ± 0.26
$\zeta/R_\star$	30.96 ± 0.45
$R_p/R_\star$	0.1134 ± 0.0020
b^2	$0.729^{+0.014}_{-0.017}$
$b \equiv a \cos i / R_\star$	$0.854^{+0.008}_{-0.010}$
i (deg)	83.6 ± 0.4
Limb-darkening coefficients [b]	
a_i (linear term, i filter)	0.1975
b_i (quadratic term)	0.3689
a_z	0.1448
b_z	0.3599
RV parameters	
K (m s^{-1})	88.1 ± 3.3
k_{RV}[c]	-0.006 ± 0.015
h_{RV}[c]	-0.027 ± 0.034
e	0.035 ± 0.024
ω (deg)	252 ± 84
HIRES RV fit rms (m s^{-1})	6.7
HDS RV fit rms (m s^{-1})	12.3
Secondary eclipse parameters	
T_s (BJD)	2455457.861 ± 0.027
$T_{s,14}$	0.0895 ± 0.0020
$T_{s,12}$	0.0236 ± 0.0077
Planetary parameters	
M_p (M_{J})	0.711 ± 0.028
R_p (R_{J})	1.340 ± 0.065
$C(M_p, R_p)$ [d]	0.07
ρ_p (g cm^{-3})	0.37 ± 0.05
$\log g_p$ (cgs)	2.99 ± 0.04
a (AU)	0.0419 ± 0.0005
T_{eq} (K)	1630 ± 42
Θ[e]	0.035 ± 0.002
F_{per} (10^9erg s^{-1} cm^{-2}) [f]	1.72 ± 0.16
F_{ap} (10^9erg s^{-1} cm^{-2}) [f]	1.49 ± 0.19
$\langle F \rangle$ (10^9erg s^{-1} cm^{-2}) [f]	1.59 ± 0.16
Parameters from Rossiter-McLaughlin Effect	
Projected spin-orbit angle, λ [deg]	73.5 ± 9.0
$v \sin i_\star$ [km s^{-1}]	3.07 ± 0.24

[a] T_c: Reference epoch of mid transit that minimizes the correlation with the orbital period. T_{14}: total transit duration, time between first to last contact; $T_{12} = T_{34}$: ingress/egress time, time between first and second, or third and fourth contact.
[b] Values for a quadratic law, adopted from the tabulations by Claret (2004) according to the spectroscopic (SME) parameters listed in Table 3.
[c] Lagrangian orbital parameters derived from the global modeling, and primarily determined by the RV data.
[d] Correlation coefficient between the planetary mass M_p and radius R_p.
[e] The Safronov number is given by $\Theta = \frac{1}{2}(V_{esc}/V_{\mathrm{orb}})^2 = (a/R_p)(M_p/M_\star)$ (see Hansen & Barman 2007).
[e] Incoming flux per unit surface area, averaged over the orbit.

Doppler-measurement code. The resulting formula for the anomalous velocity was

$$V_{\mathrm{RM}}(t) = \Delta f(t)\, v_p(t) \left[1.005 - 0.1141 \left(\frac{v_p(t)}{2.2\ \mathrm{km\ s^{-1}}} \right)^2 \right],$$
$$(2)$$

where Δf is the fraction of light blocked by the planet, and v_p is the projected rotation velocity of the portion of the star that is hidden by the planet. In calculating $\Delta f(t)$, we adopted a linear limb-darkening law. In calculating $v_p(t)$, we assumed uniform rotation around an axis that is inclined by an angle λ from the orbit normal as projected on the sky (using the same coordinate system as Ohta et al. (2005) and Fabrycky & Winn (2009)).

Most of the orbital and transit parameters are much more tightly constrained by other observations. For this reason we adopted Gaussian priors on $R_p/R_\star$, T_{12}, T_{14}, T_c, P, K, and $v \sin i_\star$, based on the mean parameter values and 1-σ uncertainties quoted in Tables 3 and 4. We also used a Gaussian prior on the linear limb-darkening coefficient to describe the spectroscopic transit, with central value 0.65 (based on an interpolation of the tables of Claret (2004)) and a standard deviation of 0.10. The only completely free parameters were λ and γ. We fitted the 58 RVs from 2011 Feb 21, adopting uncertainties equal to the quadrature sum of the internally-estimated uncertainty and a "jitter" term of 4.8 m s^{-1}, the value giving $\chi^2 = N_{\mathrm{dof}}$.

To derive parameter values and uncertainties we used a Markov Chain Monte Carlo (MCMC) algorithm employing Gibbs sampling and Metropolis-Hastings stepping. Table 4 summarizes the results for the key parameters. Figure 4 shows the RV data and the results for $v \sin i_\star$ and λ.

The result for λ is $73.5° \pm 9.0°$ degrees. The finding of a large misalignment is obvious from visual inspection of Figure 4, which shows that the anomalous RV was a blueshift throughout the entire transit, as opposed to the "red-then-blue" pattern of a well-aligned system.

The result $v \sin i_\star = 3.07 \pm 0.24$ km s^{-1} based on the RM analysis is $\sim 2\sigma$ larger than the result 2.2 ± 0.5 km s^{-1} that was derived from the observed spectral line broadening. This could be a signal of systematic errors in the spectral analysis, imperfections in our RM calibration scheme, or possibly even differential rotation (which would affect both measurements in different ways). Fortunately the result for λ is nearly immune to possible systematic errors in $v \sin i_\star$, as the errors in those two parameters are nearly uncorrelated.[12] This is true of most systems with high transit impact parameters (Gaudi & Winn 2007).

4. DISCUSSION

We have reported the discovery of HAT-P-30b, a giant planet in a close-in orbit around a late F-type dwarf star. The star is relatively bright ($V = 10.4$), which will facilitate many interesting follow-up observations, such as studies of the planet's atmosphere through transmission and occultation spectroscopy. One such follow-up study, the detection and analysis of the Rossiter-McLaughlin effect, has already been conducted and presented in this paper.

The pace of discovery of new exoplanets continues to rise each year, and the properties of this ever-larger ensemble have revealed many patterns that hint at the processes shaping the observed architectures of plane-

---

[12] When the prior constraint on $v \sin i_\star$ was released, and the analysis was repeated, the results were $\lambda = 68.9 \pm 9.8$ degrees and $v \sin i_\star = 3.39 \pm 0.33$ km s^{-1}.

tary systems. One such pattern among the transiting hot Jupiters was discovered by Winn et al. (2010) who noted a tendency for planets around hot stars to have misaligned orbits ($|\lambda| \gtrsim 10°$), while planets orbiting cool stars have orbits that are more closely aligned with the stellar rotation. This pattern also manifests itself in the statistical distribution of projected stellar rotation rates ($v \sin i_\star$). Schlaufman (2010) searched for anomalously low values of $v \sin i_\star$ among the host stars of transiting exoplanets, which would be an indication of significant spin-orbit misalignments along the line of sight (small $\sin i_\star$). Schlaufman found that many of the most massive (and hottest) planet host stars among his sample showed evidence of misalignment.

HAT-P-30b is a newly discovered hot Jupiter ($P = 2.810595 \pm 0.000005$ days, $M_p = 0.711 \pm 0.028\,M_{\mathrm{J}}$) orbiting a hot ($T_{\mathrm{eff}} = 6300$ K) host star. Our spectroscopic observations made during the transit of the planet exhibit the Rossiter-McLaughlin effect, revealing a sky-projected angle between the star's spin axis and the planet's orbit normal $\lambda = 73.5° \pm 9.0°$. The HAT-P-30 system therefore represents another example of a misaligned hot Jupiter orbiting a hot star, and conforms to the observed correlation between spin-orbit misalignment and stellar effective temperature (see also Winn et al. 2011). It has also been suggested that planet mass and orbital eccentricity are factors linked to spin-orbit misalignment (see, e.g., Johnson et al. 2009, Hébrard et al. 2010), although HAT-P-30 is not particularly massive, nor is the orbit detectably eccentric.

The reason why hot stars tend to have high obliquities is not known, but one possible factor is tidal interactions (Winn et al. 2010). As mentioned in the introduction, cool stars have thicker convective envelopes where tidal dissipation is thought to be stronger. Close-in planets might be able to torque the convective layer of cool stars into alignment, while hot stars lack massive outer convective layers and their planets remain misaligned. This scenario suggests that hot Jupiters generally arrive at their close-in orbits with substantial orbital tilts. It also requires a long-lived decoupling between the convective and radiative layers of Sun-like stars, a situation not observed in the Sun. However, the tidal-interaction model makes a clear prediction: exceptions to the T_{eff}–misalignment correlation should be found in systems containing planets with small masses or wide orbits, since the strength of tidal interactions is diminished in either case. As noted by Winn et al., the only "strong exceptions" among their sample are systems with planets in wide orbits, including WASP-8b and HD80606b (Queloz et al. 2010; Moutou et al. 2009; Winn et al. 2009). Another test is the case of the HAT-P-11 system, which contains a Neptune-mass planet ($M_P = 0.1\,M_{\mathrm{J}}$) orbiting a cool star. Indeed Winn et al. (2010) and Hirano et al. (2011) found that the planet is in a highly misaligned orbit.

Additional tests are warranted using a larger and more diverse sample of transiting planets. Fortunately, this larger sample is forthcoming since planets around bright ($V < 12$) F- and G-type stars straddling the proposed division between "hot" and "cold" ($T_{\mathrm{eff}} = 6250$ K) are in the detectability "sweet spot" of ground-based transit surveys such as HATNet.
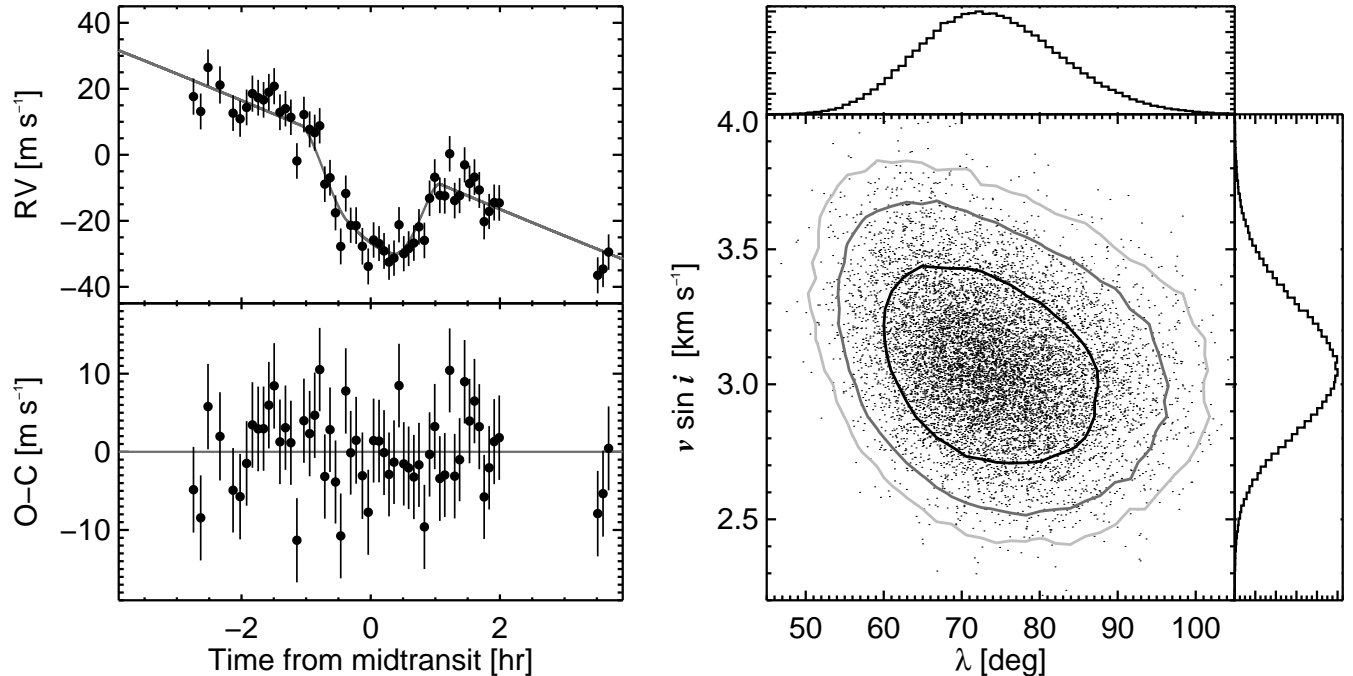
FIG. 4.— **Rossiter-McLaughlin effect for HAT-P-30** *Left.*—Apparent radial velocity variation on the night of 2011 Feb 21, spanning a transit. The top panel shows the observed RVs. The bottom panel shows the residuals between the data and the best-fitting model. *Right.*—Joint constraints on λ and $v \sin i_\star$. The contours represent 68.3%, 95.4%, and 99.73% confidence limits. The marginalized posterior probability distributions are shown on the sides of the contour plot.

REFERENCES

Anderson, D. R., et al. 2010, ApJ, 709, 159
Bakos, G. Á., Noyes, R. W., Kovács, G., Stanek, K. Z., Sasselov, D. D., & Domsa, I. 2004, PASP, 116, 266
Bakos, G. Á., et al. 2007, ApJ, 670, 826
Bakos, G. Á., et al. 2010, ApJ, 710, 1724
Borucki, W. J., et al. 2011, ApJ, 728, 117
Buchhave, L. A., et al. 2010, ApJ, submitted, arXiv:1005.2009
Butler, R. P. et al. 1996, PASP, 108, 500
Carpenter, J. M. 2001, AJ, 121, 2851
Charbonneau, D., Brown, T. M., Latham, D. W., & Mayor, M. 2000, ApJ, 529, L45
Claret, A. 2004, A&A, 428, 1001
Droege, T. F., Richmond, M. W., & Sallman, M. 2006, PASP, 118, 1666
Fabrycky, D. C., & Winn, J. N. 2009, ApJ, 696, 1230
Ph.D. thesis, University of Szeged, Hungary
Gaudi, B. S. & Winn, J. N. 2007, ApJ, 655, 550
Hansen, B. M. S., & Barman, T. 2007, ApJ, 671, 861
Henry, G. W., Marcy, G. W., Butler, R. P., & Vogt, S. S. 2000, ApJ, 529, L41
Hébrard, G., et al. 2008, A&A, 488, 763
Hébrard, G., et al. 2010, A&A, 516, A95
Hirano, T., Narita, N., Shporer, A., Sato, B., Aoki, W., & Tamura, M. 2011, PASJ, in press [arXiv:1009.5677]
Howard, A. W., et al. 2010, ApJ, 721, 1467
Isaacson, H., & Fischer, D. 2010, ApJ, 725, 875
Johnson, J. A., et al. 2008, ApJ, 686, 649

Johnson, J. A., Winn, J. N., Albrecht, S., Howard, A. W., Marcy, G. W., & Gazak, J. Z. 2009, PASP, 121, 1104
Jenkins, J. M., et al. 2010, ApJ, 724, 1108
Kovács, G., Zucker, S., & Mazeh, T. 2002, A&A, 391, 369
Kovács, G., Bakos, G. Á., & Noyes, R. W. 2005, MNRAS, 356, 557
Lin, D. N. C., & Papaloizou, J. 1986, ApJ, 309, 846
Latham, D. W., et al. 2009, ApJ, 704, 1107
Ohta, Y., Taruya, A., & Suto, Y. 2005, ApJ, 622, 1118
Pál, A., & Bakos, G. Á. 2006, PASP, 118, 1474
Pál, A. 2009b, arXiv:0906.3486, PhD thesis
Mandel, K., & Agol, E. 2002, ApJ, 580, L171
Marcy, G. W., & Butler, R. P. 1992, PASP, 104, 270
McLaughlin, D. B. 1924, ApJ, 60, 22
Morton, T. D., & Johnson, J. A. 2011, ApJ, 729, 138
Moutou, C., et al. 2009, A&A, 498, L5
Noguchi, K., et al. 2002, PASJ, 54, 855
Queloz, D., Eggenberger, A., Mayor, M., Perrier, C., Beuzit, J. L., Naef, D., Sivan, J. P., & Udry, S. 2000, A&A, 359, L13
Queloz, D., et al. 2010, A&A, 517, L1
Rossiter, R. A. 1924, ApJ, 60, 15
Sato, B., Kambe, E., Takeda, Y., Izumiura, H., & Ando, H. 2002, PASJ, 54, 873
Sato, B., et al. 2005, ApJ, 633, 465
Schlaufman, K. C. 2010, ApJ, 719, 602
Skrutskie, M. F., et al. 2006, AJ, 131, 1163
Torres, G. et al. 2007, ApJ, 666, 121
Triaud, A. H. M. J., et al. 2010, A&A, 524, A25

Valenti, J. A., & Fischer, D. A. 2005, ApJS, 159, 141
Valenti, J. A., & Piskunov, N. 1996, A&AS, 118, 595
Vaughan, A. H., Preston, G. W., & Wilson, O. C. 1978, PASP, 90, 267
Vogt, S. S. et al. 1994, Proc. SPIE, 2198, 362
Yi, S. K. et al. 2001, ApJS, 136, 417

Winn, J. N., Noyes, R. W., Holman, M. J., Charbonneau, D., Ohta, Y., Taruya, A., Suto, Y., Narita, N., Turner, E. L., Johnson, J. A., Marcy, G. W., Butler, R. P., & Vogt, S. S. 2005, ApJ, 631, 1215
Winn, J. N., et al. 2006, ApJ, 653, L69
Winn, J. N., et al. 2009, ApJ, 703, 2091
Winn, J. N., Fabrycky, D., Albrecht, S., & Johnson, J. A. 2010, ApJ, 718, L145
Winn, J. N., et al. 2010, ApJ, 723, L223
Winn, J. N., et al. 2011, AJ, 141, 63